

REACTIVITY, MAGNETISM AND LOCAL ATOMIC STRUCTURE IN FERROMAGNETIC FE LAYERS DEPOSITED ON SI(001)

N. G. GHEORGHE, M. A. HUSANU, G. A. LUNGU, R. M. COSTESCU,
D. MACOVEI, D. G. POPESCU, C. M. TEODORESCU*

*National Institute of Materials Physics, P.O. Box MG-7, Atomistilor 105b, 077125
Bucharest-Magurele, Romania*

This work presents recent studies concerning the synthesis of ultrathin ferromagnetic Fe layers on Si(001) and the correlated follow-up measurement of their structural properties, interface reactivity, and magnetism. This study is undertaken as function of the amount of Fe deposited and of substrate temperature. The interface reactivity is characterized by Auger electron spectroscopy. The surface structure is characterized by low electron energy diffraction (LEED). The local order of Fe atoms is investigated by X-ray absorption fine structure (XAFS) and the magnetism by magneto-optical Kerr effect (MOKE). A general trend established is that a higher deposition temperature stabilizes a better surface ordering, but also enhances Fe and Si interdiffusion and therefore decreases the magnetism. A surprising effect obtained by Fe deposition at room temperature is that, despite the rapid disappearance of the long range order with Fe deposition (no LEED pattern is observed for Fe coverage exceeding one monolayer), the material exhibits a significant uniaxial in-plane magnetic anisotropy. When the deposition is performed at high temperature (500 °C), a weak ferromagnetism is still observed, with saturation magnetization of about 10 % of the value obtained for room temperature deposition. The combined MOKE and EXAFS studies allowed inferring consistent values for the range of Fe thicknesses where the reaction takes place and the main properties of the distinct formed layers.

(Received February 22, 2012; Accepted March 13, 2012)

Keywords: surface magnetism; surface reactivity; metal-semiconductor interfaces; molecular beam epitaxy; XAFS; Auger electron spectroscopy

1. Introduction

Fe layers deposited on silicon have been subject of numerous investigations in the past, since this interface involves both the most common pure ferromagnetic metal and the most used semiconductor in the industry. One of the global aims of this research is to provide recipes for fabrication of ferromagnetic contacts on semiconductors for spin injection. However, spin injection efficiency is strongly dependent on the reactivity at interface. At the same time, the magnetism of the layers itself is strongly perturbed by the interface reactivity [1]. A second great interest which emerged in the study of such systems during the last years is based on the narrow direct bandgap of 0.87 eV of β -FeSi₂, together with its high optical absorption coefficient, which promote this material as suitable for solar energy conversion and light emission [2,3].

To date, extensive studies were carried out involving especially Fe/Si(111) interfaces [4] because most importantly, the Si(111) c(7×7) interface is easier to prepare than the Si(001) c(2×1) interface. Secondly, the Si(111) surface may be passivated (*e.g.* with hydrogen) and one expects a lower interface reactivity in this case [5]. It is found that the Fe reaction at the Si(111) interface is

*Corresponding author: teodorescu@infim.ro

very important. This strongly affects the magnetism of very thin layers, promoting dead silicide layers with thickness of several angstroms [6].

In this work we will address Fe/Si(001) interfaces, for which fewer studies combining reactivity with magnetism are reported to date. Synthesis of β -FeSi₂ silicide was demonstrated by medium energy ion scattering when annealing an Fe film grown on Si(001) at about 400 °C [4]. At the same time, using photoelectron spectroscopies, two plateaus were identified in the ratio between the Si 2p and Fe 3p core level intensity, corresponding to the formation of FeSi between 400 and 570 °C, and FeSi₂ between 600 and 850 °C [7]. More recent Rutherford backscattering spectroscopy studies reported the placement of Fe atoms in subsurface sites [8], with out-diffusion of Si during annealing at 300-400 °C, yielding FeSi₂ [8], result which is in line with similar findings on Fe/Si(111) [4,5]. More recent sputtering experiments produced β -FeSi₂ when depositing Fe on Si(001) heated at 500 °C, and a mixture of α -FeSi₂ and β -FeSi₂ when the substrate temperature is increased [9]. However, the surface was not properly characterized in this last experiment. A more complete structural characterization performed by low energy electron diffraction (LEED) and low energy ion scattering (LEIS) evidenced Si-terminated FeSi₂ formation with a (2×2) reconstruction when annealing at 540 °C; single crystal FeSi₂ was formed after several cycles of deposition and annealing [10]. Turning now to the magnetic properties, we mention that one decade ago it was recognized that Fe/Si(111) forms Fe stripes along <110> directions, which become easy magnetization axes [11]. A similar situation is encountered when using the Si(001) surface for deposition [6,12]. The formation of the elongated islands along <110> directions are formed by FeSi₂ [13], but little was mentioned about their magnetism. Amorphous FeSi layers provided interesting in-plane magnetic anisotropy [14].

Note also that efforts were made to inhibit the Fe-Si reaction either by using a Au buffer layer [15] or by the so-called "template method" when a buffer FeSi₂ or CoSi₂ layer is previously synthesized on Si(001), followed by the evaporation of Fe [16], since it is now largely accepted that the diffusion coefficient of Fe into FeSi₂ is considerably lower than in Si [9].

Trying to put everything together, it seems that when the Fe deposition is performed at room temperature, Si diffusion into the Fe film promotes a layer of approximate composition Fe₃Si [17], which becomes ferromagnetic for coverages exceeding 3.6 ML \approx 5 Å [15] or about 7 Å [6,18]. Note that, in any case, at 20 Å of Fe deposited the system presents well-defined spin asymmetry in the band structure [19]. At high temperature, nonmagnetic iron silicide (FeSi, FeSi₂) is formed [6]. First principle calculations predict nonmagnetic or very weak magnetism of FeSi/Si(001) [20].

The aim of this paper is to investigate the long- and short-range ordering, composition and magnetic properties of Fe deposited onto Si(001) in order to see which are the correlations between magnetic properties, interface reactivity and local atomic order. The long-range order was investigated by LEED, the chemical reactivity and intermixing by Auger electron spectroscopy (AES), the short-range neighboring of Fe by X-ray absorption fine structure (XAFS), and the magnetic properties by magneto-optical Kerr effect (MOKE).

2. Experimental

Ultrathin Fe layers were prepared on atomically clean Si(001) in a molecular beam epitaxy chamber (manufacturer: Specs GmbH, Germany) operating in the pressure range of low 10⁻¹⁰ mbar. The samples are investigated *in situ* by Auger electron spectroscopy (AES), low-energy electron diffraction (LEED), and reflection high energy electron diffraction (RHEED).

Single crystals of Si(001) were cleaned by 2-3 cycles of heating Si(001) wafers at 1200 °C for 30 minutes in a vacuum not exceeding 1×10⁻⁹ mbar, then waiting for the vacuum to recover back to low 10⁻¹⁰ mbar [21]. Figure 1 presents AES survey spectra of the as-prepared Si(001), where one may notice also a very fast contamination (within ~ 30 min) under the electron beam of the Auger spectrometer even at the measuring pressure of 10⁻⁹ mbar [21,22]. However, the estimated maximum contamination level for the as-prepared Si(001) is ~ 0.2 % of a single atomic layer of C contamination and below 0.1 % of a single layer for O contamination. Also, bright (1×2)-(2×1) spots are observed for the as-prepared sample [Fig. 2(a)]. However, the observation of

(1×2)-(2×1) LEED spots is demonstrated in Ref. [21] to not suffice in demonstrating the sample cleanliness. Therefore, X-ray photoelectron spectroscopy (XPS) was used to further check the sample cleanliness and it was demonstrated that, indeed, the above preparation procedure yields to a very low degree of contamination (below 10^{-3} of a single atomic layer) [21].

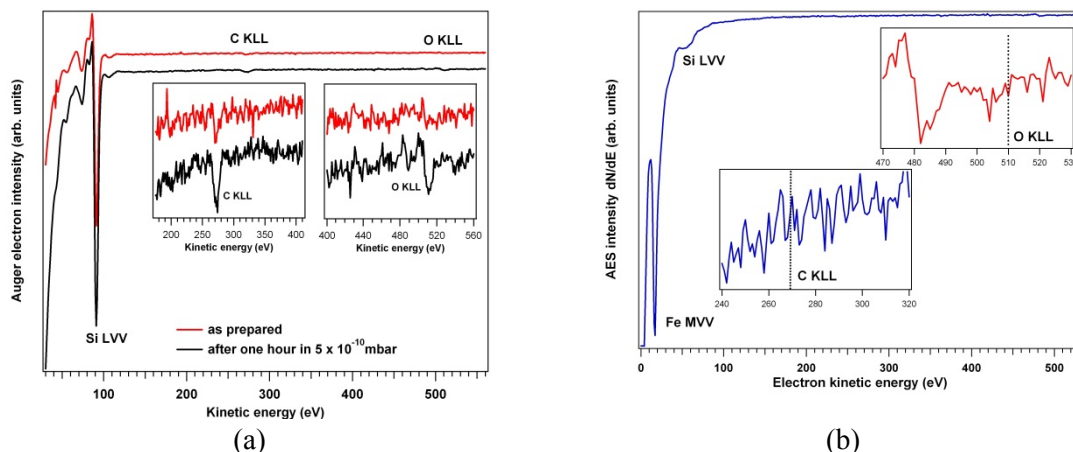


Fig. 1. Survey scans of Auger electron spectroscopy (a) on the as-prepared Si(001) sample and (b) on a layer of 6.7 nm Fe immediately after deposition on Si(001).

Fe was evaporated from a Specs EBE-4 electron bombardment source at a rate of 0.06 \AA/s and at normal incidence. The base pressure was in the $1\text{-}2 \times 10^{-9}$ mbar range during deposition. In the following, we shall refer to the Fe coverage as related to bulk *bcc* Fe. 1 monolayer (ML) of Fe is equivalent to $\sim 1.43 \text{ \AA}$, as indicated by the thickness monitor set with Fe parameters (density, *Z*-factor). The Fe coverage was also *a posteriori* checked with AES signal intensities. The residual gas was monitored during deposition and was composed of about 80 % hydrogen. Therefore, no contamination was detected after Fe deposition, as it may be seen from Fig. 1(b).

After the deposition, the samples are capped with 3 nm of Au and characterized *ex situ* by MOKE, using a setup manufactured by AMACC Anderberg and Mod er Accelerator AB. The maximum applied field is 0.6 T and the measurements are performed at room temperature. Moreover, the setup allows azimuthal rotation of the sample in order to investigate the longitudinal Kerr effect along several in-plane crystallographic directions. The same capped samples were transported to the Hasylab synchrotron radiation facility, where they were analyzed by X-ray absorption fine structure: extended X-ray absorption fine structure (EXAFS) and X-ray absorption near-edge spectroscopy (XANES) at the Fe K-edge (7112 eV) on the A1 beamline. The EXAFS data analysis was performed by using custom made software which was found to be fully compatible with *Athena*.

3. Results and discussions

3.1. Structure and long range order

Figure 2 presents the evolution of LEED patterns when the deposition is achieved at an elevated temperature ($500 \text{ }^\circ\text{C}$). The as-prepared sample exhibits well-defined (2×1) and (1×2) reconstructions. As soon as Fe is deposited, the LEED pattern weakens and broadens. For 2.8 \AA deposited, which represents roughly 2 single atomic layers of Fe, only a broad (1×1) pattern is visible. For the equivalent of 6 Fe layers (Fig. 2c), the spots are barely visible; however, they seem to become narrower. A detailed spot profile analysis yielded the lateral size of the islands formed as being $\sim 20 \text{ nm}$ for the Fe coverage corresponding to the equivalent of 6 single atomic layers [23].

When the deposition is performed at room temperature, the LEED pattern disappears for the lowest quantity of Fe deposited, 0.7 \AA , which roughly corresponds to half a monolayer. By considering the coherence length of $\sim 25 \text{ nm}$ corresponding to electrons of around 50 eV kinetic energy [5], this implies that at room temperature deposition islands with considerable lower lateral

dimension are formed on the surface, with increasing surface roughness on the same order of magnitude. No LEED pattern was visible at energies of 100 eV either, where the coherence length is about 18 nm. Therefore, the formation of islands of some 20×50 nm, as reported in Ref. [13], may be ruled out by the present observation. If islands are formed, their typical size is of about 10 nm or lower.

Consequently, as reported in several previous publications [1,9,10,16], room temperature deposition of metal on silicon (or onto other single crystal semiconductors) leads to rough interfaces even for amounts of metal not exceeding one single atomic layer. Heating the substrate improves the long range ordering in most cases [1] but, as it will be seen below, this induces formation of silicides that are almost epitaxially grown on the clean semiconductor substrate.

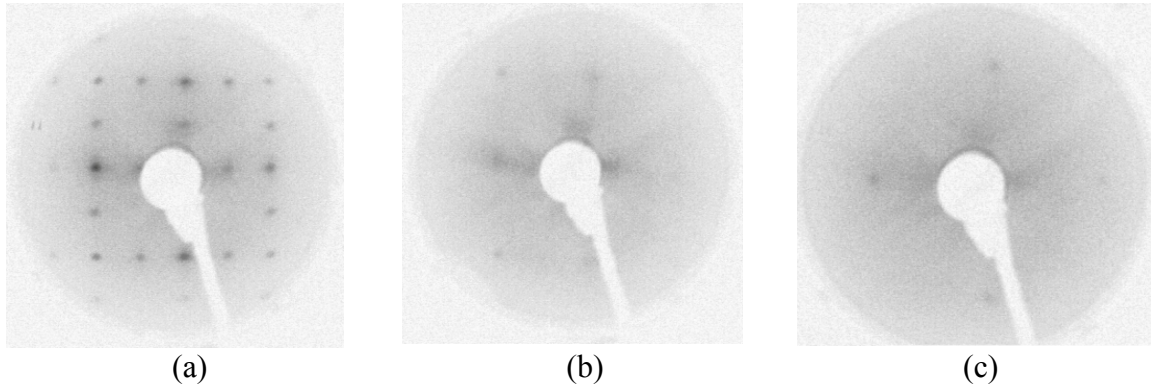


Fig. 2. Evolution of LEED patterns with Fe deposition at 500 °C. (a): clean Si(001); (b): 2.1 Å deposited; (c): 8.4 Å Fe/Si(001). For a better visualization, negatives of the photographs are represented.

3.2. Intermixing and reactivity at the interface

Figure 3 presents Auger electron spectroscopy (AES) results obtained from the Si LVV and Fe MVV lines for (a) samples where the deposition took place at room temperature and (b) the samples synthesized at high temperature (500 °C). In the following, we will use the following two formulas for the AES data:

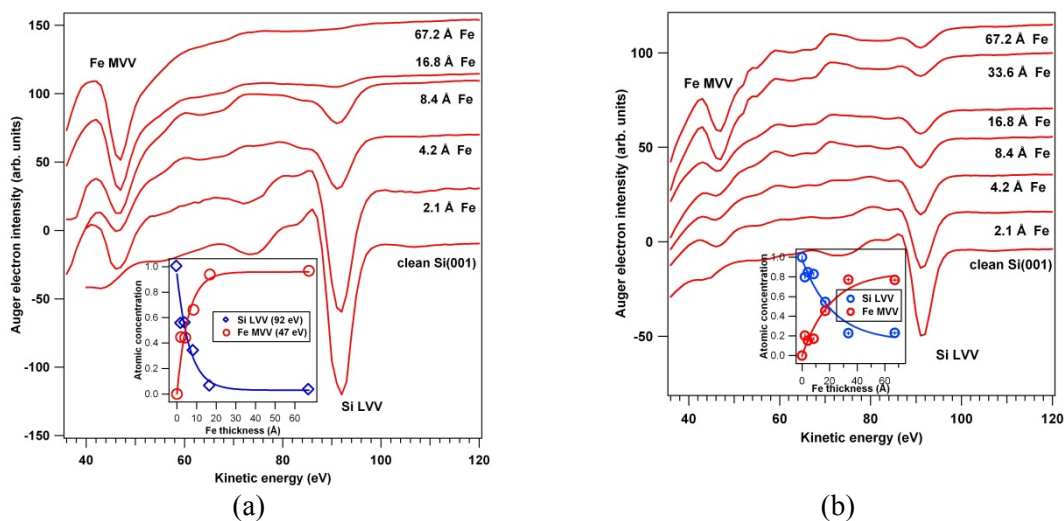


Fig. 3. Auger electron spectra for Si LVV and Fe MVV: (a) the room temperature deposition; (b) the deposition performed at 500 °C substrate temperature. The inserts represent thickness dependencies on the Fe coverage, together with fits using eq. (1) for the Si signal and eq. (2) for the Fe signal. The AES intensities from the insert were corrected by the Auger sensitivity factors.

- for the substrate (Si) signal:

$$I_{Si}(\theta) = A_{Si} \exp(-\theta / \lambda_{Si}) + B_{Si} \quad (1)$$

where θ is the Fe coverage, A_{Si} is the bulk Si intensity and B_{Si} any remaining Si signal accounting for Si atoms diluted or reacted with the Fe layer near the sample surface. λ_{Si} is the inelastic mean free path (IMFP) of Si Auger electrons.

- for the overlayer (Fe) signal:

$$I_{Fe}(\theta) = A_{Fe} [1 - \exp(-\theta / \lambda_{Fe})] \quad (2)$$

where A_{Fe} is the bulk Fe intensity and λ_{Fe} is the IMFP of Fe Auger electrons. The electron IMFP is estimated at λ_{Si} (~ 92 eV) $\approx \lambda_{Fe}$ (~ 47 eV) $\approx 6 \pm 1.5$ Å [24].

The Si LVV and Fe MVV signals were corrected by the Auger sensitivity factors from the MultiPak AES database distributed by Physical Electronics. In this database, values are tabulated for the Auger differential intensities for excitation energies of 3, 5 and 10 keV. In our experiments, a lower excitation energy of 1.1 keV was used in order to prevent damage and reduce electron-induced sample contamination [22]. The AES sensitivity factors for 1.1 keV were obtained by polynomial extrapolation of the above mentioned data. AES factors of 0.880 for Si LVV and of 0.398 for Fe MVV resulted from this extrapolation. Therefore, the raw AES intensities were corrected by these factors; furthermore, a normalization was applied so that the resulting Fe + Si signal stayed constant, since no other atoms (C, O, etc.) were detected by AES. This normalization accounts for instabilities of the incident electron beam from one experiment to another and for possible changes in measurement geometry (small mechanical imperfections of the feedthroughs). It is very important for this normalization that the Auger electron inelastic mean free path to be nearly the same, which was assumed for Si LVV and Fe MVV. This was checked after the data analysis (see Table 1). Consequently, one extracts 'experimental' atomic concentrations which are plotted in the inserts of Fig. 3. We will designate these curves as 'apparent' compositions. Furthermore, the data were fitted with the functions (1) and (2) defined above. The resulting fitting parameters are synthesized in Table 1.

It may be noticed that, for the room temperature deposition [Fig. 3(a)], the IMFPs λ_{Si} and λ_{Fe} are close enough and also close to the accepted values for this energy range [24]. Consequently, in this case, one may infer that the Fe layer is situated over the Si substrate and that low intermixing occurs. There are some Si atoms diffused into the Fe layer. Assuming that these Si atoms are uniformly distributed into the Fe layer and that the amplitude A_{Fe} represents the Fe signal coming from an Fe layer of equivalent thickness λ_{Fe} (without taking into account electron IMFP effects), the concentration of these diffused Si atoms will be given by $B_{Si}/A_{Fe} \approx 3.13 \pm 0.34$ %. Assuming that all of these Si atoms are just floating at the sample surface, as it was reported in Ref. [10], their surface concentration is given by $(B_{Si}/A_{Fe}) \times (\lambda_{Fe} / 1.4 \text{ Å}) \approx 12.9 \pm 1.4$ %. In any case, the formation of a nearly unreacted Fe layer is observed by this technique. The two extreme cases are (i) ~ 3 % Si uniformly diffused in the Fe layer or (ii) some 13 % of a single atomic layer of Si located at the surface.

Table 1. Fitting parameters extracted from the 'apparent' compositional data (Fig. 4) fitted with formulas (1) and (2).

Parameter	A_{Si} (%)	B_{Si} (%)	λ_{Si} (Å)	A_{Fe} (%)	λ_{Fe} (Å)
RT deposition	92 ± 0.5	3 ± 0.3	6.45 ± 0.17	96 ± 0.7	5.78 ± 0.14
500 °C deposition	83 ± 0.8	15 ± 0.8	22.1 ± 1.2	85 ± 1	20.8 ± 1.1

For the high temperature (500 °C) case represented in Fig. 3(b), the situation changes dramatically: the Si signal is attenuated following a law like (1) but with a much larger IMFP (22.1 Å). At the same time, a considerable Si signal is present after the thick Fe film deposition.

Assuming that a compound of constant stoichiometry is formed and applying the same considerations as in the previous paragraph, the resulting Si concentration is $B_{\text{Si}}/A_{\text{Fe}} \approx 17.6 \pm 1.1$ %. An approximate stoichiometry of Fe_6Si or Fe_5Si is then derived for this layer, which may be formed by 2-3 parts Fe and one part Fe_3Si , to introduce here the compound reported in several previous works [6,15,17-19]. The fact that at this temperature Fe and Si are reacting is not a novelty in view of everything described in the Introduction. The novelty here is the relatively low concentration of Si in the intermixed layer (about one half of what one expects from a homogenous Fe_3Si compound) obtained in the present experiment. Maybe the difference was the lower Fe deposition rate than in previously reported experiments: 0.06 \AA/s as compared with the typical rate of about 1 \AA/s used by most other studies [14]. Accordingly, one might expect also that some enhanced magnetic properties may be exhibited by these reacted layers.

3.3. Local atomic order

Figure 4 presents the X-ray absorption near-edge spectra (XANES) of bulk *bcc* Fe, of a pressed pellet of FeSi_2 powder and of two 6.7 nm thick films, prepared at room temperature or at $500 \text{ }^\circ\text{C}$ substrate deposition temperature, both capped with Au layers. It may be seen that a gradual departure from the Fe spectrum is presented by the room-temperature film, and then a further departure is presented by the film obtained at high temperature. Nevertheless, the FeSi_2 -like spectrum is never reached even by this latter curve.

In the following, we will consider that the pre-edge feature is connected to the $1s \rightarrow 3d$ dipole forbidden transition and its intensity is related to the number of Fe 3d vacancies [25]. A proof of this attribution is the increase by a factor of ~ 2 in intensity in the pre-edge feature (which in fact becomes the main edge) in FeSi_2 (Fig. 5) with respect to metal Fe. This implies that the 3d holes are twice as numerous in FeSi_2 as in Fe, so one may infer that the $4s^1 3d^7$ configuration of metal Fe becomes $4s^0 3d^4$; hence 4 electrons for each Fe are hybridizing with the Si 3p orbitals in ionocovalent (spd) bindings.

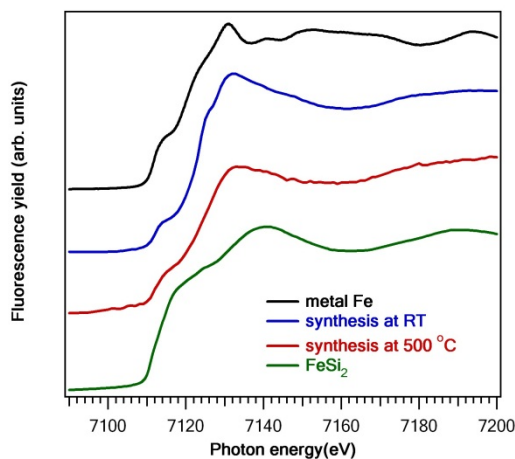


Fig. 4. X-ray absorption near edge structure (XANES) of metal Fe, of reference FeSi_2 and of $\text{Fe/Si}(001)$ deposited at room temperature and at high temperature.

The decrease (by a factor of ~ 1.5) in the pre-edge feature for $\text{Fe/Si}(001)$ synthesized at room temperature may also be connected to a decrease of the Fe 3d density of unfilled states. It is unlikely to be able to attribute this decrease to an enrichment of the Fe 3d population, but rather to the observed disorder of this film. Possibly, the Au overlayer also transfers electrons towards the Fe film, diminishing the number of 3d vacancies. At the same time, this pre-edge feature is more prominent and perhaps its overall integrated intensity is not decreasing. However, for the sample synthesized at high temperature, where more severe intermixing of Si and Fe was observed by

AES, the intensity of the pre-edge peak increases again, proving that 3d electrons have been transferred towards silicon.

The oscillations of the absorption after the edge have considerable fewer structures in the Fe/Si(001) samples, as compared with bulk Fe. This is in line with the observed character of the surface evolution by LEED, where the long range order disappears. However, this observation by XAFS reinforces the preeminent amorphous character of the films, whereas from LEED we could just comment on the lower limit of the long range ordering domains. The weak extended X-ray absorption fine structure (EXAFS) signal was extracted and Fourier transformed using a Hanning window, following the standard procedure of the EXAFS data analysis described in Ref. [26].

The Fourier transforms (FTs) of the EXAFS functions are given in Figure 5(a). Note the close resemblance between the FT of the bulk Fe EXAFS and already reported data [14]. At the same time, the experimental FT of the FeSi₂ EXAFS does not fit entirely with the simulation presented in Ref. [14]. The EXAFS data for the Fe/Si(001) sample synthesized at room temperature exhibits a peak related to Fe-Fe coordinations and another peak at considerable lower interatomic distance (~ 1.5 Å), which we attribute to Fe-Si bonds. Let us remark that the 'apparent' interatomic distances (R) from the FT plots [Fig. 5(a)] are not true interatomic distances, since they are affected by the slope of the dependence on the photoelectron wavevector on the phase shifts involved in the EXAFS function: the backscattering phase shift $\varphi_j(k)$ and the absorbing atom phase shift $\delta_i'(k)$. Indeed, the Si scattering phase shift has a much steeper dependence on k in the range of low values of k than the Fe scattering phase shift, and this produces the large difference in the FT peak values. Similar values were observed in Ref. [14] as well. In fact, one may express the observed 'apparent' interatomic distance as $R_{j,\text{obs}} \approx R_j + (1/2) \partial\varphi/\partial k \equiv R_j + \Delta R$, where φ is the total pair phase (absorbing atom + backscatterer). These pair phases are represented in Fig. 5(b). The average value for ΔR in the case of the Fe-Fe pair (Fe absorber + Fe scatterer) is $\langle\Delta R\rangle = -0.33$ Å. Consequently, the true first order interatomic distance is the sum of the observed value for bulk Fe for the first maximum in the FT (2.15 Å) + the corresponding ΔR . This yields 2.54 Å, which compares well (within 2 %) with the real value of 2.49 Å. For the Fe-Si pair in FeSi₂, $\langle\Delta R\rangle = -0.45$ Å and the observed maximum of the FT corresponding to the first coordination shell occurs at 1.94, which yields a real distance of 2.39 Å, essentially the same as that often reported in literature for β -FeSi₂ phase grown on Si single crystals [9,10,27].

The FT of the Fe/Si(001) present a main peak located at $\sim 1.565 \pm 0.015$ Å. Applying, further, the $\langle\Delta R\rangle = -0.45$ Å correction discussed previously results in a 'real' Fe-Si distance of 2.015 Å, considerably lower than the Fe-Si distance in FeSi₂. Thus, the Fe silicide films are strongly distorted and one cannot speak of the formation of β -FeSi₂ in any of the cases of Fe/Si(001) analyzed here. In turn, $2.015 \text{ \AA} \approx a_{\text{Fe}}/2^{1/2}$, where $a_{\text{Fe}} \approx 2.872$ Å. This suggests that interdiffused Si atoms start to place in the centers of the *bcc* Fe elementary cell, converting this structure to a NaCl one, where the 1:1 Si:Fe stoichiometry is attained. Therefore, in the case of high temperature synthesis, a mixture of Fe-Fe and Fe-Si is observed, with a considerably higher amount of Fe-Si and perhaps the formation of a NaCl-like FeSi compound.

A quantitative analysis is difficult to perform at this moment. The correct way to interpret the data is to perform a Fourier filtering, backtransform in k space and perform a nonlinear fit of the data, where the average number of neighbors and the interatomic distances may be derived more accurately. This is a difficult task firstly because the actual data statistics was not appropriate. Instead, one may do just an evaluation as follows: the ratio between the Fe-Si and the Fe-Fe peak amplitude in the FT is 1.85 for the sample synthesized at room temperature. This ratio increases to 3.48 for the sample synthesized at high temperature. Therefore, there are about 1.9 more Fe-Si bonds formed at high temperature than at room temperature. Assuming that this number of bonds is proportional to the number of Si atoms (for low Si concentrations), it means that the Si concentration in the sample prepared at 500 °C is, roughly, almost twice the concentration in the sample prepared at room temperature, whereas from AES considerations this ratio equals $17.6 \% / 3.13 \% \approx 5.6$. Here we may argue that, as discussed above, the AES has a limited surface sensitivity of $\sim 3\lambda \sim 20$ Å, whereas the fluorescence detection of the XAFS signal essentially investigates with similar sensitivity the whole Fe film (the Fe K radiation used for detection is at about 6.4 keV). Therefore, such a difference may originate from an increased

concentration of Si in the inner Fe(Si) films formed after deposition. This phenomenon may happen in both films and the AES data just investigate the outer layers towards the surface.

It is therefore tempting to do an evaluation of the Si/Fe ratio based only on the EXAFS data. If, for simplicity, one considers for FeSi the NaCl structure, there are twelve first order (Si) neighbors of Fe, whereas in *bcc* Fe the first (Fe) first order neighbors are only eight. The FT maxima must scale with this number of neighbors, given the fact that the scattering amplitudes are comparable [see insert in Fig. 6(b)]. Therefore, in a FeSi-like environment Fe is roughly more abundant than the Fe in a *bcc* Fe environment by a factor of $1.85/(12/8) \approx 1.23$. Therefore, the room-temperature deposited sample of equivalent Fe thickness of 6.7 nm might be seen in a first approximation as being composed of about $6.7 \times 1.23 / 2.23 \approx 3.7$ nm reacted Fe with Si, with subsequent growth of a (disordered) Fe layer of ~ 3 nm with a *bcc* Fe-like environment. This does not contradict the AES data obtained for the thick film (6.7 nm), since the FeSi layer signal is completely damped by a factor of $\exp(-3 \text{ nm} / 6 \text{ \AA}) = \exp(-5) = 6.7 \times 10^{-3}$.

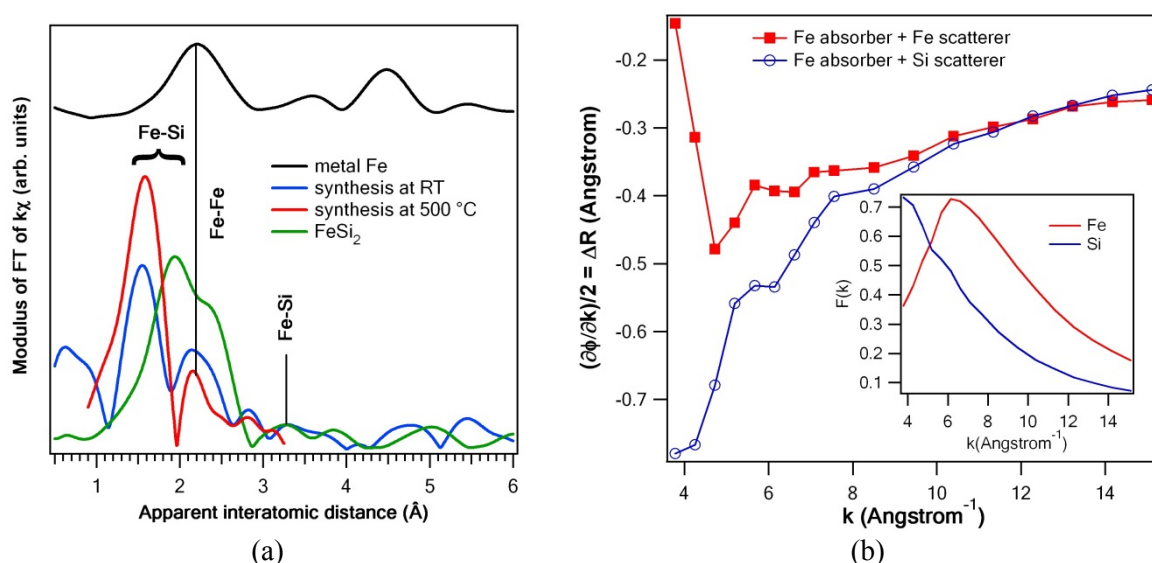


Fig. 5 (a) Fourier transforms of the EXAFS functions for 7 nm Fe layers grown either at room temperature or at high temperature on Si(001), compared with the corresponding signal obtained from a metal Fe foil. (b) Theoretical EXAFS phase shifts, computed from the data in Ref. [26]. Inserted: theoretical Fe and Si backscattering amplitudes.

The same analysis performed on the sample synthesized at 500 °C, based on the EXAFS data, yields a factor of 2.32 between Fe in a FeSi environment and Fe in environments similar to bulk *bcc* Fe. Therefore, one obtains that roughly 2 nm of Fe are synthesized in bulk Fe form and the remaining part of the equivalent 4.7 nm of bulk *bcc* Fe forms FeSi. The formation of FeSi₂ may be ruled out, since the corresponding Fourier transform is really too different from the one obtained from the thin film deposited. Formation of other silicides may also be proposed, but in the absence of a standard spectrum we cannot argue any further on this hypothesis.

These assumptions will be cross-checked in the following Subsection, correlated with the magnetic properties of these films.

3.4. Magnetic properties

We now address the magnetic properties of these layers and interfaces, by means of magneto-optical Kerr effect (MOKE) measurements. Figure 6 represents MOKE hysteresis loops obtained in both cases discussed above (different deposition temperatures). As may be seen from Fig. 6(a), for samples synthesized at room temperature a detectable MOKE signal is observed. Moreover, this signal is different when the applied magnetic field is parallel to one of the $\langle 100 \rangle$ or to $\langle 110 \rangle$ directions. In other words, an *uniaxial magnetic anisotropy* is observed, although this sample did not exhibit any long range order. The Fe nanoparticles formed whose lateral

dimensions are below 20 nm, according to the considerations of § 3.1, are, however, in well defined positions with respect to the the crystallographic axes of the substrate. For a long time it was believed that only Fe/GaAs(001) exhibits uniaxial magnetic anisotropy [28] and only recently the same phenomenon was reported for Fe/Si(001) [14,16]. The present results strengthen the hypothesis that the uniaxial magnetic anisotropy observed is independent of the atomic nature of the semiconductor; moreover, we demonstrate clearly that the uniaxial magnetic anisotropy occurs even when long range ordering is absent.

Experiments on Fe/Ge(001) have identified uniaxial magnetic anisotropies [29], but these anisotropies were shown to depend on the substrate preparation: especially the bulklike uniaxial magnetic anisotropy was shown to be related to the preparation conditions of the sample, in particular the oblique sputtering on Ge substrate before Fe deposition and the oblique deposition of the Fe film. Similar uniaxial magnetic anisotropy depending on the preparation condition was shown for Co/Cu(001) [30] or Fe/MgO(001) [31]. Typically, the easy axis was shown to be perpendicular to the plane of incidence. In Ref. [32], Fe is deposited onto a pre-formed $c(4\times 8)$ flat iron silicide layer. No uniaxial magnetic anisotropy was found when the deposition was performed at normal incidence, but just when the deposition was performed at oblique incidence. This was correlated with STM images showing the formation of elongated structures in the direction perpendicular to the Fe beam. However, in the present experiment the deposition was performed at normal incidence, so we may rather draw the conclusion that the uniaxial magnetic anisotropy is rather a property of the interface, as in Ref. [14], than induced by the deposition conditions.

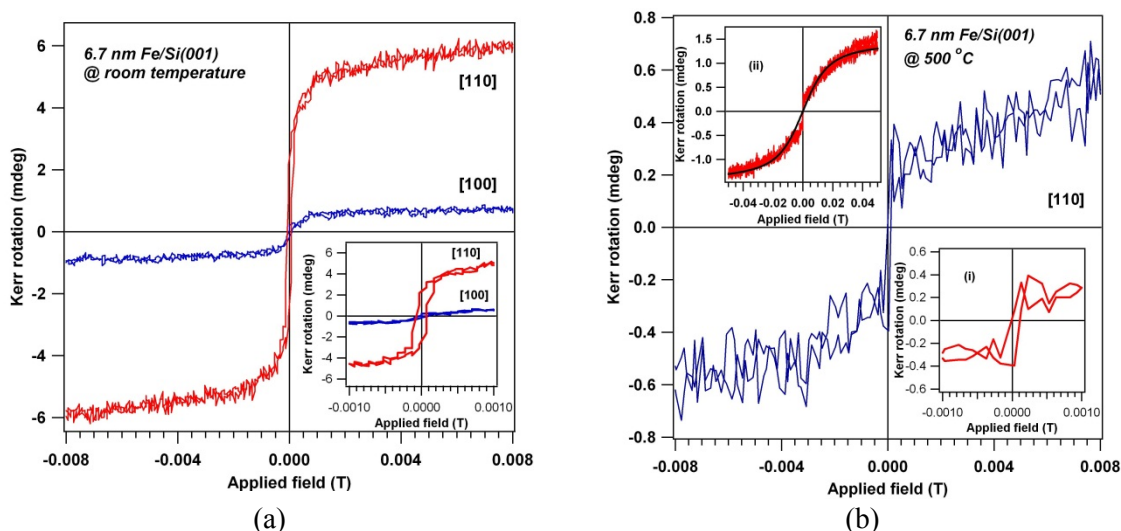


Fig. 6. MOKE hysteresis loops obtained on the samples synthesized at room temperature (a) and at 500 °C (b). For the former case, hysteresis loops when applying the magnetic field along two surface high symmetry directions are shown. The insert in (a) and insert (i) in (b) presents a zoom around zero applied field. Insert (ii) in (b) presents the extended region in order to emphasize the superparamagnetic behavior.

We now evaluate the strength of the Fe atomic momentum. In Ref. [15], a longitudinal Kerr signal of some $100 \mu\text{rad} \approx 5.7 \text{ mdeg}$ is reported for about 13 ML $\approx 1.9 \text{ nm}$ of Fe deposited on Si(001) when an Au buffer layer is employed in order to inhibit the reaction. Additionally, by using exactly the same setup as the one in the present study, a MOKE saturation signal of $\sim 10 \text{ mdeg}$ is obtained for 5 nm of bulk Fe deposited [33]. Consequently, we infer that $2.5 \pm 0.5 \text{ mdeg}$ of MOKE signal corresponds to 1 nm of an Fe layer, where the Fe magnetic moment is $2.2 \mu_B$ (Bohr magnetons). Coming now to our study, in the case of room temperature deposition we obtained about 6 mdeg of MOKE signal, which corresponds to $2.4 \pm 0.6 \text{ nm}$ metal Fe layers. This is in line with the obtained value from the primary analysis of the EXAFS signal by Fourier transform (about 3 nm). Consequently, we may infer that the Fe layer detected by EXAFS is highly likely magnetic and the Fe average magnetic moment in this layer is close to the bulk value

of $2.2 \mu_B$, or perhaps slightly less ($1.8-1.9 \mu_B$). This value is quite similar to the reported value of Fe layers on GaAs(001) or InAs(001), once the interface reaction ends [1].

The same analysis may be applied to the sample synthesized at 500°C [Fig. 6(b)]. Here the saturation MOKE signal is one order of magnitude lower than at room temperature, whereas the estimated bulklike Fe layer (from XAFS) is about 2 nm. Therefore, an average Fe atomic magnetic momentum of about $0.12 \pm 0.03 \mu_B$ is obtained in this case. This is about 5.4 % of the bulk Fe magnetic momentum. Therefore, we might infer that by depositing at high temperature some Fe is still magnetic, but with a very low magnetic momentum.

Another point to be mentioned concerns the superparamagnetic behavior of this film. The insert (ii) in Fig. 6(b) presents magnetometry results over a wider range of applied fields B_a (in Tesla). This signal was fitted with the Brillouin formula:

$$B_J(B_a) = \text{Const.} \times \left[\frac{2J+1}{2J} \coth\left(\frac{2J+1}{2J} \frac{g\mu_B J B_a}{k_B T}\right) - \frac{1}{2J} \coth\left(\frac{1}{2J} \frac{g\mu_B J B_a}{k_B T}\right) \right] \quad (3)$$

where g is the gyromagnetic factor and $k_B T$ the Boltzmann term. Fitting the magnetization curve with the Brillouin function yields the value of the total momentum per superparamagnetic nanoparticle J and thus one may evaluate its (magnetic) size. It turned out that $J \sim 33,000$, and therefore there are some 22,000 Fe atoms in a nanoparticle. Now, the typical size of such nanoparticle may be approximated as being constituted by $22 \times 22 \times 22$ unit cells, *i.e.* by a cube with an edge of about 6.3 nm. We mention again that a diffuse LEED was still visible in this case, with electrons at about 50 eV kinetic energy, and that the coherence length was estimated at around 25 nm. Obviously, the nanoislands assumed above could not produce a LEED pattern. Therefore, we go to the other extreme case and estimate the thickness of such a nanoparticle if its typical dimension parallel to the (001) substrate plane is $\sim 25 \times 25 \text{ nm}^2$. It is found that this thickness value is about 5 nm, which is consistent with the derived value of 4.7 nm of equivalent Fe thickness of the reacted layer from EXAFS. Therefore, the superparamagnetic particles seem to be formed by Fe reacted with silicon rather than by the remaining unreacted Fe atoms.

4. Conclusions

New results are reported concerning the long range order, interface reactivity, and magnetic properties of Fe/Si(001). By growing at room temperature no long range order is detected; however, these small metal Fe particles exhibit noticeable ferromagnetism and uniaxial magnetic anisotropy. Also, no superparamagnetism of these moieties is obtained and the coercitive field is very low, about $0.75 \pm 0.05 \text{ Oe}$, in line with the reported properties of amorphous Fe layers obtained by magnetron sputtering in Ref. [14]. When the growth is performed at higher temperatures, Fe reacts completely with Si forming a long range ordered Fe silicide with weak, though detectable, ferromagnetism.

It is clear that further investigations (particularly by MFM and by depth profiling assisted by X-ray photoelectron spectroscopy) are needed in order to fully clarify these magnetic properties. Part of these experiments are in preparation now and will be subject of a separate publication. For now we will conclude with two rather crude models, as follows: (i) When Fe is deposited at room temperature, about one half of the Fe atoms are reacting with silicon, producing a compound that exhibits very weak magnetism or is nonmagnetic, whereas the other half of Fe atoms produce a an Fe film with Fe magnetic moment close to the bulk value. Although this film does not present any long range crystalline order, it presents uniaxial magnetic anisotropy with the easy axis along the substrate $\langle 110 \rangle$ orientation. This result may look surprising, but a similar finding was reported some years ago in Ref. [14]. The Si interdiffusion into the Fe layer is very weak, a few (3-4) atomic percents. (ii) When Fe is deposited at 500°C , the amount of unreacted Fe layer diminishes and, also, its magnetic moment decreases by a factor of almost 20. This may be connected to a considerable higher amount of Si diffused into Fe (about 18 atomic %), as seen by Auger electron spectroscopy. Such strong damping of the long range ferromagnetic order was also reported in Fe-rich silicides, *e.g.* in Fe_3Si [14], but, to date, not any in phases so rich in Fe.

This low thickness layer with strong Si interdiffusion (equivalent to Fe_{5.7}Si) covers another layer (built from about two thirds of the deposited Fe), constituted by islands of an FeSi compound with superparamagnetic behavior, which also is a quite new result.

This study constitutes one of the rare ones combining MBE deposition with *in situ* AES and LEED characterization, and with *ex situ* magnetic and local order investigations by XAFS. We believe that the facts presented here will contribute to the elucidation of the interface formation in the highly studied Fe/Si(001) system.

Acknowledgements

Support from the HasyLab beamline scientist Dr. Edmund Welter is gratefully acknowledged. This work is funded by the Romanian National Authority for Scientific Research under the CNCSIS Grant PCCE-ID_76. One of the authors (RMC) is supported by the Romanian re-integration grant RP11/2009.

References

- [1] C. Teodorescu, F. Chevrier, V. Ilakovac, O. Heckmann, L. Lechevalier, R. Brochier, R.L. Johnson, K. Hricovini, Appl. Surf. Sci. **166**, 137 (2000); C.M. Teodorescu, F. Chevrier, R. Brochier, C. Richter, O. Heckmann, V. Ilakovac, P. De Padova, K. Hricovini, Surf. Sci. **482-485**, 1004 (2001); C.M. Teodorescu, F. Chevrier, R. Brochier, V. Ilakovac, O. Heckmann, L. Lechevalier, K. Hricovini, Eur. Phys. J. B **28**, 305 (2002); M. Izquierdo, M. E. Dávila, J. Avila, H. Ascolani, C. M. Teodorescu, M. G. Martin, N. Franco, J. Chrost, A. Arranz, M. C. Asensio, Phys. Rev. Lett. **94** (2005) 187601; C.M. Teodorescu, D. Luca, Surf. Sci. **600**, 4200 (2006).
- [2] Y. Makita, Y. Nakayama, Y. Fukuzawa, S.N. Wang, N. Otagawa, Y. Suzuki, Z.X. Liu, M. Osamura, T. Ootsuka, T. Mise, H. Tanoue, Thin Solid Films **461**, 202 (2004).
- [3] K. Konuma, J. Vrijmoeth, P.M. Zagwijn, J.W.M. Frenken, E. Vlieg, J.F. van der Veen, J. Appl. Phys. **73**, 1104 (1993).
- [4] A. Mascaraque, J. Avila, C.M. Teodorescu, M.C. Asensio, E.G. Michel, Phys. Rev. B. **55**, R7315 (1997); J. Avila, A. Mascaraque, C. Teodorescu, E.G. Michel, M.C. Asensio, Surf. Sci. **377-379**, 856 (1997).
- [5] M.G. Martin, J. Avila, M. Gruyters, C. Teodorescu, P. Dumas, Y.J. Chabal, M.C. Asensio, Appl. Surf. Science **123-124**, 156 (1998).
- [6] I.I. Pronin, M.V. Gomoyunova, D.E. Malygin, D.V. Vyalikh, Y.S. Dedkov, S.L. Molodsov, J. Appl. Phys. **104**, 104914 (2008).
- [7] J. Alvarez, J.J. Hinarejos, E.G. Michel, G.R. Castro, R. Miranda, Phys. Rev. B **45**, 14042 (1992).
- [8] K. Kinoshita, R. Imaizumi, K. Nakajima, M. Suzuki, K. Kimura, Thin Solid Films **461**, 131 (2004).
- [9] M. Itakura, D. Norizumi, T. Ohta, Y. Tomokiyo, N. Kuwano, Thin Solid Films **461**, 120 (2004).
- [10] F. Shoji, H. Shimoji, Y. Makihara, M. Naitoh, Thin Solid Films **461**, 116 (2004).
- [11] M. Cougo dos Santos, J. Geshev, J.E. Schmidt, S.R. Teixeira, L.G. Pereira, Phys. Rev. B **61**, 1311 (2000).
- [12] B. Ghebouli, S.M. Chérif, A. ayadi, B. Helifa, M. Boudissa, J. Magn. Magn. Mater. **312**, 194 (2007).
- [13] M. Suzuki, K. Kinoshita, S. Jomori, H. Harada, K. Nakajima, K. Kimura, Thin Solid Films **515**, 8281 (2007).
- [14] J. Diaz, S.M. Valvidares, R. Morales, J.M. Alameda, J. Magn. Magn. Mater. **242**, 166 (2002).
- [15] F. Zavaliche, W. Wulfhekel, H. Xu, J. Kirschner, J. Appl. Phys. **88**, 5289 (2000).
- [16] P. Bertoncini, P. Wetzel, D. Berling, G. Gewinner, C.U. Bouillet, V. P. Bohnes, Phys. Rev. B **60**, 11123 (1999); P. Bertoncini, P. Wetzel, D. Berling, A. Mehdaoui, B. Loegel,

- G. Gewinner, R. Poinso, V.P. Bohnes, *J. Magn. Magn. Mater.* **237**, 191 (2001).
- [17] J.M. Gallego, J.M. García, J. Alvarez, R. Miranda, *Phys. Rev. B* **46**, 13339 (1992).
- [18] I.I. Pronin, M.V. Gomoyunova, D.E. Malygin, D.V. Vyalikh, Y.S. Dedkov, S.L. Molodtsov, *Appl. Phys. A* **94**, 467 (2009).
- [19] R. Kläsger, C. Carbone, W. Eberhardt, C. Pampuch, O. Rader, T. Kachel, W. Gudat, *Phys. Rev. B* **56**, 10801 (1997).
- [20] J.I. Lee, I.G. Kim, *J. Magn. Magn. Mater.* **272** (2004) 1186; H. Wu, P. Kratzer, M. Scheffler, *Phys. Rev. B* **72**, 144425 (2005).
- [21] N.G. Gheorghe, G.A. Lungu, R.M. Costescu, C.M. Teodorescu, *Phys. Stat. Solidi B* **248**, 1919 (2011); N.G. Gheorghe, G.A. Lungu, R.M. Costescu, D.G. Popescu, C.M. Teodorescu, *Optoelectron. Adv. Mater. - Rapid Comm.* **5**, 499 (2011).
- [22] J. Xu, W.J. Choyke, J.T. Tales Jr., *J. Appl. Phys.* **82**, 6289 (1997).
- [23] N.G. Gheorghe, M.A. Husanu, G.A. Lungu, R.M. Costescu, D. Macovei, C.M. Teodorescu, *J. Mater. Sci.* **47**, 1614 (2012).
- [24] S. Hüfner, *Photoelectron spectroscopy. Principles and applications*, 3rd Ed., Springer, Berlin, 2003.
- [25] D. Mardare, V. Nica, C.M. Teodorescu, and D. Macovei, *Surf. Science* **601**, 4479 (2007).
- [26] B.K. Teo, *EXAFS: Basic Principles and Data Analysis*, Springer, Berlin, 1983.
- [27] H.S. Zeng, X. Wallart, J.P. Nys, G. Dalmai, P. Friedel, *Phys. Rev. B* **44**, 13811 (1991).
- [28] G.A. Prinz, *Science* **250**, **1092** (1990); M. Gester, C. Daboo, R.J. Hicken, S.J. Gray, A. Ercole, J.A.C. Bland, *J. Appl. Phys.* **80**, 347 (1996).
- [29] M. Cantoni, M. Riva, R. Bertacco, F. Ciccacci, *Phys. Rev. B* **74**, 134415 (2006).
- [30] S. van Dijken, G. Di Santo, B. Poelsema, *Phys. Rev.* **63**, 104431 (2001).
- [31] J.H. Wolfe, R.K. Kawakami, W.L. Ling, Z.Q. Qiu, R. Arias, D. L. Mills, *J. Magn. Magn. Mater.* **232**, 36 (2001).
- [32] G. Garreau, J.L. Bubendorff, S. Hajjar, D. Berling, S. Zabroki, A. Mehdaoui, R. Stephan, P. Wetzel, G. Gewinner, C. Pirri, *phys. stat. sol. (c)* **1**, 3726 (2004).
- [33] V. Kuncser, W. Keune, U. von Hörsten, G. Schinteie, *J. Optoelectron. Adv. Mater.* **12**, 1385 (2010).